Nonlinear elasticity of ε -Fe: The pressure effect

O. M. Krasilnikov,[1] A. V. Lugovskoy,[2,3] V. Dikan,[2,4] M. P. Belov,[2] Yu. Kh. Vekilov,[1,2] and I. A. Abrikosov[2,5]
[1]*Department of Theoretical Physics and Quantum Technologies, NUST "MISIS", RU-119991 Moscow, Russia*
[2]*Materials Modeling and Development Laboratory, NUST "MISIS", RU-119991 Moscow, Russia*
[3]*Institute for Molecules and Materials, Radboud University, Heijendaalseweg 135, NL-6525 AJ Nijmegen, The Netherlands*
[4]*Instituto de Ciencia de Materiales de Barcelona (ICMAB-CSIC), Campus de Bellaterra, 08193 Barcelona, Spain*
[5]*Department of Physics (IFM), Linkoping University, SE-58183 Linkoping, Sweden*

(Received 26 April 2018; revised manuscript received 5 November 2018; published 7 May 2019)

Description of elasticity of iron at the ultrahigh pressures is a challenging task for physics, with a potential strong impact on other branches of science. In the present work, we calculate the elastic properties of *hcp* iron in the pressure range of 50–340 GPa beyond the linear elasticity approximation, conventionally assumed in theoretical studies. We define the higher order elastic constants and present expressions for the long-wave acoustic modes Grüneisen parameters of a compressed *hcp* crystal. We obtain the second and third order elastic constants of the *hcp* Fe in the considered pressure interval, as well as its Grüneisen parameters for the high-symmetry directions. The latter are directly compared with the Grüneisen parameters derived from the volume dependences of the vibrational frequencies calculated in the quasiharmonic approximation. The obtained results are used for the stability analysis of the *hcp* phase of iron at high pressures.

DOI: 10.1103/PhysRevB.99.184101

I. INTRODUCTION

The pressure in the Earth's inner core, which consists mainly of Fe reaches 330–360 GPa, There is numerous evidence that the ε phase of iron with hexagonal closed packed (*hcp*) structure [1–4] is stable at such extreme compression at low-to-intermediate temperature. Thus, a knowledge of elastic properties of this phase is crucial for many reasons, e.g., for the interpretation of seismic observations [5]. Consequently, the elastic properties of ε-Fe were studied in many experimental and theoretical works. According to the experimental data [3,4], a transition from *bcc* Fe to *hcp* structure at room temperature takes place at 10–18 GPa. Magnetic properties of the *hcp* Fe are still under discussion [6]. However, it is generally accepted that at room temperature the *hcp* phase is nonmagnetic at least at pressures exceeding 50 GPa and has a wide stability interval, predicted theoretically to extend at least to 5700 GPa [7], and confirmed experimentally to at least 400 GPa [8]. Several experimental studies of elastic properties were performed on polycrystalline samples of epsilon Fe and at different pressures, including the radial x-ray diffraction experiments (RXD) [9,10], inelastic x-ray scattering (IXS) [11,12], and Raman spectroscopy [13]. From these experiments, the second order elastic constants (SOECs) of single crystals were derived. Theoretical studies of SOECs of monocrystalline *hcp* iron in the pressure interval up to 400 GPa were performed using density functional theory (DFT) [14–18].

However, the second order elastic constants characterize the linear elastic response. To the best of our knowledge, the higher order elastic constants of Fe, like the third order elastic constants (TOECs) are not known, and therefore their prediction is of interest. TOECs reflect the anharmonicity of lattice vibrations and define the lowest order of nonlinear response. They are important for the understanding of anharmonic properties of solids, such as thermal expansion, Grüneisen parameters, dependences of elastic responses, and sound velocities on temperature and applied pressure, among others [19,20]. Moreover, TOECs determine the wave-form distortion of ultrasonic finite-amplitude waves passing through a solid, as well as an amplitude of the second harmonic wave [21,22].

In the present work we employ a technique of higher order elastic constants calculations for compressed crystals [23,24]. The full set of SOECs and TOECs of ε-Fe in the pressure interval 50–340 GPa is calculated at temperature $T = 0$ K. The DFT is used for the calculations of energy at different volumes and deformations. The expression for the Grüneisen parameters of long-wave acoustic modes of *hcp* crystals using the second and third order elastic constants is given. We calculate these parameters for longitudinal and transverse acoustic modes for high-symmetry directions in the considered pressure interval. For comparison, we calculated the phonon dispersion relations and derived the Grüneisen parameters from the volume dependences of vibrational frequencies. The obtained results were used for the analyses of stability of the *hcp* phase of iron at high pressure.

The paper is organized as follows. In Sec. II we define the second and higher order elastic constants for a compressed crystal. The method of their calculation and the details of the employed *ab initio* technique are presented in Secs. III and IV. Section V presents the analysis of the calculated SOECs, TOECs, and vibrational properties of the *hcp* Fe, followed by conclusions.

II. DEFINITION OF HIGHER ORDER ELASTIC CONSTANTS OF A LOADED CRYSTAL

The nth order elastic constants ($n \geqslant 2$) of a compressed crystal characterize the elastic response of a material on a

finite deformation under hydrostatic pressure. Let us define the initial (compressed, but undeformed) state as the equilibrium state at the given temperature and external pressure, while the deformed state is the one under the effect to an additional, generally nonhydrostatic strain. We characterize the deformed state using the Lagrangian tensor of finite deformations η_{ij} [19]:

$$\eta_{ij} = \tfrac{1}{2}(\alpha_{ki}\alpha_{kj} - \delta_{ij}), \tag{1}$$

where $\alpha_{kj} = \partial r_k/\partial R_j$ is the deformation gradient, r_k and R_j are the Cartesian coordinates of point of solid in the deformed and the initial states, respectively, and δ_{ij} is the Kronecker delta. Note that we use the Einstein summation convention for the summation over the repeated indexes.

The Gibbs free energy G can be expanded in Tailor series over components of the deformation tensor η_{ij}:

$$\frac{\Delta G}{V_0} = \frac{1}{2!}\tilde{C}_{ijkl}\eta_{ij}\eta_{kl} + \frac{1}{3!}\tilde{C}_{ijklmn}\eta_{ij}\eta_{kl}\eta_{mn} + \ldots, \tag{2}$$

where $\Delta G = G(P,T,\eta) - G(P,T,0)$ is the change of thermodynamic potential upon deformation η_{ij} and V_0 is the volume of the system in the initial state (note that this is the volume at pressure P rather than the equilibrium volume at $P = 0$ GPa). In Eq. (2) we introduce the isothermal elastic constants of the nth order ($n \geqslant 2$) of the loaded crystal [23]:

$$\tilde{C}_{ijkl\ldots} = \frac{1}{V_0}\left(\frac{\partial^n G}{\partial\eta_{ij}\partial\eta_{kl}\ldots}\right)_{T,\eta=0}. \tag{3}$$

At a fixed hydrostatic pressure P the change of the Gibbs free energy upon the change of volume can be expressed as

$$\frac{\Delta G}{V_0} = \frac{\Delta F}{V_0} + P\frac{\Delta V}{V_0}, \tag{4}$$

where $\Delta F = F(P,T,\eta) - F(P,T,0)$ and $\Delta V = V - V_0$ are the changes of the Helmholtz free energy and the crystal volume due to the deformation η_{ij}, respectively. Thus, in Eq. (3), both the change of the free energy and the work against the external load due to the additional small deformation η_{ij} are taken into account. This is the main difference between the elastic constants of the loaded and unloaded crystal [19,25]. Elastic constants for the unloaded state are given by the relation [26]

$$C_{ijkl\ldots} = \frac{1}{V_0}\left(\frac{\partial^n F}{\partial\eta_{ij}\partial\eta_{kl}\ldots}\right)_{T,\eta=0}. \tag{5}$$

In contrast to the elastic constants defined in Eq. (5), the Cauchy relations are not fulfilled for $\tilde{C}_{ijkl\ldots}$ due to the consideration of the external pressure, the full Voigt symmetry of indexes permutation is conserved only at the hydrostatic pressure, while it is absent at other types of loads [19,25].

In the case of the adiabatic elastic constants of the compressed crystal all the above-mentioned considerations are preserved. The elastic constants are defined by the derivatives of the enthalpy H over the deformation components η_{ij} at constant entropy S [23]. Note, that for $\tilde{C}_{ijkl}$ all the expressions of the elasticity theory, including Christoffel equations, the Born rule of mechanical stability, and stress-strain relations have the same form as in the absence of the load [19,27].

III. CALCULATION OF SOECs AND TOECs FOR *hcp* CRYSTAL AT HYDROSTATIC PRESSURE

Using Eqs. (3)–(5), we express $\tilde{C}_{ijkl\ldots}$ via the derivatives of the free energy F and pressure P. We expand $\Delta F/V_0$ at a given P in the series over deformation tensor components up to the third order

$$\frac{\Delta F}{V_0} = \frac{\Delta F_1}{V_0} + \frac{\Delta F_2}{V_0} + \frac{\Delta F_3}{V_0}. \tag{6}$$

The expressions for $\frac{\Delta F_{1-3}}{V_0}$ are given in Appendix A [Eqs. (A1)–(A3)].

The volume of the studied system in the deformed state is given by the expression $V = JV_0$, where $J = \det|\alpha_{ij}|$ [19], then $\Delta V/V_0 = J - 1$. Let us express α_{ij} in terms of η_{kl}. For this purpose, we write α_{ij} as

$$\alpha_{ij} = \delta_{ij} + u_{ij}, \tag{7a}$$

where $u_{ij} = \partial u_i/\partial R_j$ ($u_i = r_i - R_i$). Then using Eq. (1) we write

$$\eta_{ij} = \tfrac{1}{2}(u_{ij} + u_{ji} + u_{ki}u_{kj}). \tag{7b}$$

Since the energy of the crystal does not depend on the rotation of the crystal "as a whole," we consider here the case of the "pure" deformation, without any rotation. In this case $\eta_{ij} = u_{ij} + \frac{1}{2}u_{ki}u_{kj}$ and $u_{ij} = \eta_{ij} - \frac{1}{2}u_{ki}u_{kj}$. Substituting this expression in Eq. (7a) and neglecting the terms, which are higher than the third order terms we obtain

$$\alpha_{ij} = \delta_{ij} + \eta_{ij} - \tfrac{1}{2}\eta_{ki}\eta_{kj} + \tfrac{1}{2}\eta_{rk}\eta_{ri}\eta_{kj}. \tag{8}$$

Using Eq. (8), it is possible to express J via the components of η. The expressions are given in Appendix B.

Using Eqs. (3), (4), (6), (A1)–(A3) and expressions for $\Delta V/V_0$, Eqs. (B1)–(B4), as well as combining the expressions with the same set of deformation components, we obtain the relations between $\tilde{C}_{\alpha\beta..}$ and $C_{\alpha\beta..}$, given in Table I.

Thus, for calculations of the elastic constants of compressed crystals we need to find elastic constants $C_{\alpha\beta..}$ corresponding to the volume V_0 and the pressure P from the dependence of the Helmholtz free energy F on the finite deformations tensor components η_{ij} [see Eqs. (A1)–(A3)], followed by the determination of $\tilde{C}_{\alpha\beta..}$ using relations from Table I.

In Refs. [14–18] SOECs at V_0 corresponding to pressure P were calculated using Eq. (5) with the condition of constant (in the second order over η) atomic volume, which requires a special choice of deformed states. This approach is not applicable in the calculation of the third and higher order ECs (the atomic volume should be constant in the third and higher

TABLE I. The relations between $\tilde{C}_{\alpha\beta..}$ and $C_{\alpha\beta..}$ for *hcp* crystal

$\tilde{C}_{\alpha\beta}$	$\tilde{C}_{\alpha\beta\gamma}$	
$\tilde{C}_{11} = C_{11} - P$	$\tilde{C}_{111} = C_{111} + 3P$	$\tilde{C}_{144} = C_{144} - P$
$\tilde{C}_{12} = C_{12} + P$	$\tilde{C}_{112} = C_{112} - P$	$\tilde{C}_{155} = C_{155} + P$
$\tilde{C}_{13} = C_{13} + P$	$\tilde{C}_{113} = C_{113} - P$	$\tilde{C}_{222} = C_{222} + 3P$
$\tilde{C}_{33} = C_{33} - P$	$\tilde{C}_{123} = C_{123} + P$	$\tilde{C}_{333} = C_{333} + 3P$
$\tilde{C}_{44} = C_{44} - P$	$\tilde{C}_{133} = C_{133} - P$	$\tilde{C}_{344} = C_{344} + P$

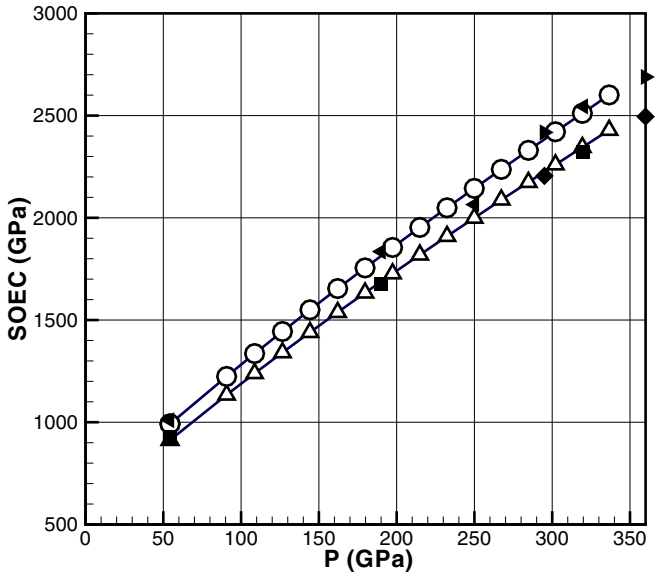

FIG. 1. Pressure dependences of elastic constants $\tilde{C}_{11}$ and $\tilde{C}_{33}$ of *hcp*-Fe calculated $T = 0$ K. $\tilde{C}_{11}$ calculated in this work are denoted with open triangles. Squares denote calculations from Refs. [14,43], diamonds denote calculations from Refs. [16,18]; $\tilde{C}_{33}$ calculated in this work are denoted with open circles, right triangles show calculations of Refs. [14,43], left triangles denote calculations of Refs. [16,18].

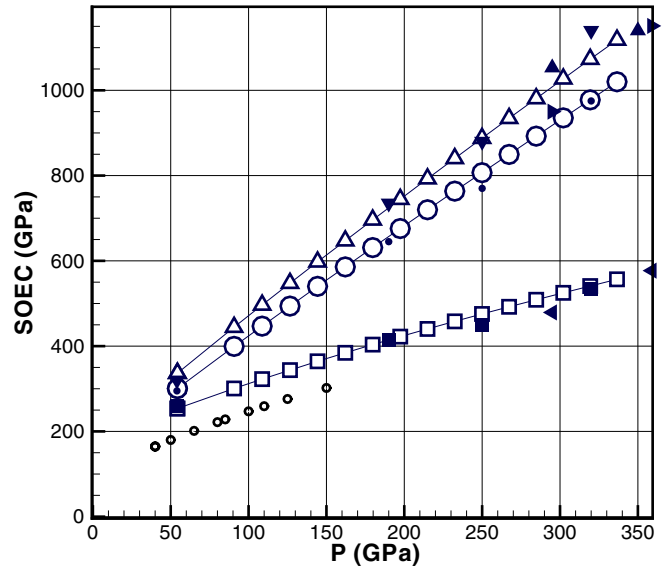

FIG. 2. Pressure dependence of elastic constants $\tilde{C}_{12}$, $\tilde{C}_{13}$, and $\tilde{C}_{44}$ of *hcp*-Fe calculated at $T = 0$ K. $\tilde{C}_{12}$ calculated in this work are denoted with open triangles. Filled down-triangles denote calculations from Refs. [14,43], filled up triangles denote calculations from Refs [16,18]; $\tilde{C}_{13}$ calculated in this work are denoted with open circles, small filled circles show calculations of Refs [14,43] right triangles show calculations of Refs. [16,18]; $\tilde{C}_{44}$ calculated in this work are denoted with open squares, black squares show calculations of Refs [14,43], left triangles are calculations from Refs. [16,18], open points show the room temperature experimental data of Refs. [13].

order over η), since the choice of the required number of such states is almost impossible.

The presented method has several advantages. First, Eq. (3) gives a unified definition of the elastic constants: the elastic constants are the nth order derivatives of the characteristic functions, which are the thermodynamic potentials at the given conditions. Second, the full set of elastic constants of required order at given P is found from the dependence of the free energy F (and from the internal energy for the adiabatic elastic constants) on deformation. Arbitrarily deformed states can be considered since the volume conservation is not mandatory. Finally, the equation of state can be obtained simultaneously with the elastic constants. As it is seen from Figs. 1 and 2, the results of our SOEC calculations at the different pressures are in a good agreement with the data obtained under the condition of volume conserving distortions.

IV. DETAILS OF CALCULATIONS

We assume that the initial (undistorted) state of a crystal at pressure P has volume V_0. To find five SOECs and ten TOECs from Eqs. (A1)–(A3) we need to consider at least ten different deformations of the *hcp* crystal. Various simple deformations and the corresponding combinations of the elastic constants are given in Table II. Here we use the following notations: $\Delta F_2/V_0 = \frac{1}{2}A\eta^2$ and $\Delta F_3/V_0 = \frac{1}{6}B\eta^3$.

TABLE II. The coefficients A and B for the different deformations of *hcp* crystal.

No.	Deformation[a]	A	B
1	$\eta_1 = \eta$	C_{11}	C_{111}
2	$\eta_3 = \eta$	C_{33}	C_{333}
3	$\eta_1 = -\eta_2 = \eta$	$2(C_{11} - C_{12})$	$4(C_{111} - C_{222})$
4	$\eta_1 = \eta_3 = \eta$	$C_{11} + 2C_{13} + C_{33}$	$C_{111} + 3C_{133} + C_{333} + 3C_{113}$
5	$\eta_6 = 2\eta$	$2(C_{11} - C_{12})$	–
6	$\eta_4 = 2\eta$	$4C_{44}$	–
7	$\eta_1 = -\eta_3 = \eta$	$C_{11} - 2C_{13} + C_{33}$	$C_{111} - 3C_{113} + 3C_{133} - C_{333}$
8	$\eta_1 = \eta_2 = \eta$	$2(C_{11} + C_{12})$	$4C_{111} + 6C_{112} - 2C_{222}$
9	$\eta_3 = \eta, \eta_6 = 2\eta$	$2(C_{11} - C_{12}) + C_{33}$	$C_{333} + 6C_{113} - 6C_{123}$
10	$\eta_1 = \eta, \eta_4 = 2\eta$	$C_{11} + 4C_{44}$	$C_{111} + 12C_{144}$
11	$\eta_2 = \eta, \eta_4 = 2\eta$	$C_{11} + 4C_{44}$	$C_{222} + 12C_{155}$
12	$\eta_3 = \eta, \eta_4 = 2\eta$	$C_{33} + 4C_{44}$	$C_{333} + 12C_{344}$

[a]Other components of the deformation tensor are equal to zero.

TABLE III. The equation of state and SOECs of the *hcp*-Fe at various pressures ($T = 0$ K). Pressures and elastic constants are given in GPa.

V_0, Å^3	P	B	$\tilde{C}_{11}$	$\tilde{C}_{12}$	$\tilde{C}_{13}$	$\tilde{C}_{33}$	$\tilde{C}_{44}$
8.886	54.30	521.1	912.5	336.5	300.6	991.6	253.7
			576[a]	307[a]	324[a]	539[a]	237[a]
			599(33)[b]	403(20)[b]	318(22)[b]	650(45)[b]	187(40)[b]
8.354	90.70	664.1	1134	444.5	399.4	1224	300.7
7.954	126.6	799.4	1341	547.6	493.9	1444	343.7
7.639	162.1	929.5	1538	647.2	585.8	1654	384.3
7.366	197.4	1055	1727	744.6	675.8	1855	422.3
7.138	232.4	1178	1910	840.2	763.5	2049	458.1
6.939	267.3	1297	2088	934.4	849.6	2237	492.3
6.764	302.1	1415	2260	1027	935.3	2421	525
6.683	319.4	1473	2345	1073	977.6	2511	540.9
6.607	336.6	1530	2429	1118	1020	2601	556.7

[a]Experiment [12]. Radial x-ray diffraction (RXD). $P = 52$ GPa. $T = 300$ K
[b]Experiment [12]. Inelastic x-ray scattering (IXS+EOS). $P = 52$ GPa. $T = 300$ K

The lattice vectors in the deformed state are given by the relation $r_i = \alpha_{ij} R_j$, where the deformation gradient α_{ij} is expressed via the Lagrangian finite deformations tensor using Eq. (8). The total energy calculations of *hcp*-Fe ($T = 0$ K) at different values of V_0 and η_{ij} were performed in the framework of the DFT as implemented in the VASP code [30]. Pressure and the elastic constants were found using the least squares fit to the total energies calculated for 30 points with 0.003 step in the range of $\eta = \pm 0.045$ from Eq. (6) and Table II.

The exchange and correlation effects were considered using the generalized gradient approximation (GGA) with PW91 parametrization [31]. The projector augmented wave (PAW) method, as implemented in VASP code, was used to consider the electron-ion interaction [32]. The integration over the Brillouin zone (BZ) was performed using the k points set with the $28 \times 28 \times 18$ points mesh, obtained by the Monkhorst-Pack method [33]. The mesh centering and reduction of the k- point number in the z direction were done in accordance with the crystal symmetry. The cut-off energy was set to 600 eV. All initial configurations of the compressed crystals were optimized with respect to the c/a lattice parameters ratio. The Methfessel-Paxton algorithm [34] with broadening 0.2 eV was used for the structure optimization. The tetrahedron method for the BZ integration with Blöchl corrections [35] was applied for the total energy calculations. A detailed description of the computational scheme and convergence issues of the used methodology can be found in Ref. [24].

For the calculations of the phonon dispersion relations, we employed the density functional perturbation theory as implemented in software package QUANTUM ESPRESSO [36,37]. We used $3 \times 3 \times 3$ uniform q-point grid resulting in six dynamical matrices. For these calculations we also used the PAW [32] potential Fe.pbe-spn-kjpaw_psl.0.2.1.UPF. The exchange and correlation effects were considered using the GGA with Perdew-Burke-Ernzerhof parametrization [38]. The integration over the BZ was performed using the k points set with the $20 \times 20 \times 13$ points mesh, obtained by the Monkhorst-Pack method [33]. The Methfessel-Paxton algorithm [34] with broadening 0.05 Ry ensured the convergence of Grüneisen parameters to 0.04 at a given k-point mesh. The cut-off energy was set to 110 Ry. The fully relaxed cells were used at all considered volumes to ensure the hydrostatic pressure conditions.

V. RESULTS AND DISCUSSION

The calculated equation of state and pressure dependence of the SOECs for ε-Fe at are summarized in Table III. Here V_0 is the volume per atom at pressure P, B is the bulk modulus defined for *hcp* structure by the relation [39]

$$B = \frac{\tilde{C}_{33}(\tilde{C}_{11} + \tilde{C}_{12}) - 2\tilde{C}_{13}^2}{\tilde{C}_{11} + \tilde{C}_{12} + 2\tilde{C}_{33} - 4\tilde{C}_{13}}. \tag{9}$$

Our calculated equation of state is in good agreement with earlier DFT calculations [14,17]. The mechanical stability requirements for the *hcp* lattice are [39]

$$\tilde{C}_{11} \geqslant |\tilde{C}_{12}|, \quad \tilde{C}_{33}(\tilde{C}_{11} + \tilde{C}_{12}) \geqslant 2(\tilde{C}_{13})^2,$$
$$\tilde{C}_{11}\tilde{C}_{33} \geqslant (\tilde{C}_{13})^2, \quad \tilde{C}_{44} \geqslant 0.$$

Our calculations show that they are fulfilled for *hcp* Fe in the whole range of pressure studied in this work.

The isotropy conditions for crystals with the hexagonal symmetry are as follows [39]: $\tilde{C}_{11} = \tilde{C}_{33}$, $\tilde{C}_{12} = \tilde{C}_{13}$ and $\tilde{C}_{11} - \tilde{C}_{12} = 2\tilde{C}_{44}$. From Table III one calculates that even at the highest pressure considered in this work $P = 336$ GPa $\tilde{C}_{33}/\tilde{C}_{11} = 1.071$, $\tilde{C}_{12}/\tilde{C}_{13} = 1.096$, $(\tilde{C}_{11} - \tilde{C}_{12})/(2\tilde{C}_{44}) = 1.177$, indicating that ε-Fe is quite isotropic. In fact, the isotropy varies very little with pressure.

Assuming central interatomic forces (independent of angle), and ions at the centers of symmetry, one arrives at the Cauchy relations for the elastic constants of hexagonal closed-packed lattice for the SOECs and TOECs [39,40]:

$$C_{12} = C_{66}, \quad C_{11} = 3C_{12}, \quad C_{13} = C_{44}, \quad C_{122} = C_{266},$$
$$C_{112} = C_{166}, \quad C_{113} = C_{155} \text{ and } C_{123} = C_{144} = C_{366} = C_{456}.$$

Note that $C_{\alpha\beta}$ and $C_{\alpha\beta\gamma}$ are defined by Eq. (5) and do not include the pressure correction. The expressions for $C_{122}, C_{166}, C_{266}, C_{366}, C_{456}$ are given in Appendix C, Eq. (C4). Using the data for SOECs and TOECs from Tables III and IV, as well as the relations between $\tilde{C}_{\alpha\beta.}$ and

TABLE IV. TOECs of the *hcp* Fe at various pressures ($T = 0$ K). All values are given in 10^{-1} GPa.

P	$-\tilde{C}_{111}$	$-\tilde{C}_{222}$	$-\tilde{C}_{333}$	$-\tilde{C}_{112}$	$-\tilde{C}_{113}$	$-\tilde{C}_{123}$	$-\tilde{C}_{133}$	$-\tilde{C}_{144}$	$-\tilde{C}_{155}$	$-\tilde{C}_{344}$
54.30	1021	918.5	919.6	118.1	99.71	18.95	201.2	47.01	135.2	220.1
90.70	1231	1105	1103	144.2	124.4	19.69	245.8	57.73	161.6	266.3
126.6	1424	1277	1280	169.2	145.9	19.73	286.8	67.46	186.0	308.3
162.1	1603	1436	1440	193.0	167.7	20.05	326.1	76.70	209.0	348.0
197.4	1772	1586	1590	215.9	188.8	21.39	363.8	85.45	231.0	385.9
232.4	1934	1728	1733	237.1	209.5	22.43	399.0	93.81	252.3	423.0
267.3	2089	1865	1872	256.7	229.8	23.47	433.3	102.0	273.1	460.0
302.1	2243	2001	2012	274.8	249.4	24.56	466.9	110.0	293.3	497.2
319.4	2318	2066	2082	284.0	259.4	25.27	483.8	114.0	303.3	516.0
336.6	2392	2130	2152	293.0	269.2	25.68	501.2	118.0	313.4	535.0

$C_{\alpha\beta}$. from Table I, we obtain the following ratios between the elastic constants at $P = 336$ GPa: $C_{11}/3C_{12} = 1.18$, $C_{66}/C_{12} = 1.27$, $C_{44}/C_{13} = 1.31$, $C_{266}/C_{122} = 1.20$, $C_{166}/C_{112} = 1.39$, $C_{155}/C_{113} = 1.47$, $C_{144}/C_{123} = 1.42$, $C_{456}/C_{366} = 1.49$. The calculated ratios depend very little on pressure and show that the Cauchy relations for ε-Fe fulfilled better for SOECs than for TOECs.

Though the calculations reproduce well the experimental pressure dependences of SOECs, their absolute values are different (see Table III, the second line). The largest disagreement is observed for $\tilde{C}_{11}$ and $\tilde{C}_{33}$ (for other elastic constants this difference is much smaller). The discrepancy is well known [14–18] and reflects certain limitations of the DFT calculations. It has been recently shown that by including correlation effects one improves the description of the equation of state of ε-Fe [41]. On the other hand, one should remember that the high-pressure experiments (the scattering or diffraction of x rays under nonhydrostatic pressure [12]) are carried out on polycrystalline samples of ε-Fe. Thus, the experimental elastic constants of single crystals are not extracted directly, and the extraction is not a straightforward task [10,42]. The discrepancy between the experimental values measured in different experiments (see Table III), can be considered as the indication of this.

The pressure dependences of the elastic constants $\tilde{C}_{\alpha\beta}$ are shown in Figs. 1 and 2. Earlier first principles calculations are also shown in the figures for comparison. It is seen that our results are in a good agreement with the data from the literature, confirming the numerical reliability of the proposed computational scheme. All five SOECs increase monotonously with pressure. Interestingly, $\tilde{C}_{11}$ and $\tilde{C}_{33}$ follow each other quite closely, while $\tilde{C}_{12}$ follows $\tilde{C}_{13}$. At the same time, the variation of $\tilde{C}_{44}$ with P is much weaker than for other elastic constants. In addition, Fig. 2 shows elastic modulus $\tilde{C}_{44}$ of ε-*Fe* and its pressure dependence, which were deduced from Raman measurements using the phenomenological three-body force model for the *hcp* solid with a nonideal c/a ratio [13,44]. It is shown that the experimental and theoretical pressure dependences of $\tilde{C}_{44}$ are similar, although the absolute values are different (∼15–20%).

Table IV and Figs. 3 –5 show TOECs for *hcp* Fe calculated at $T = 0$ K. It is seen that all TOECs are negative. Their

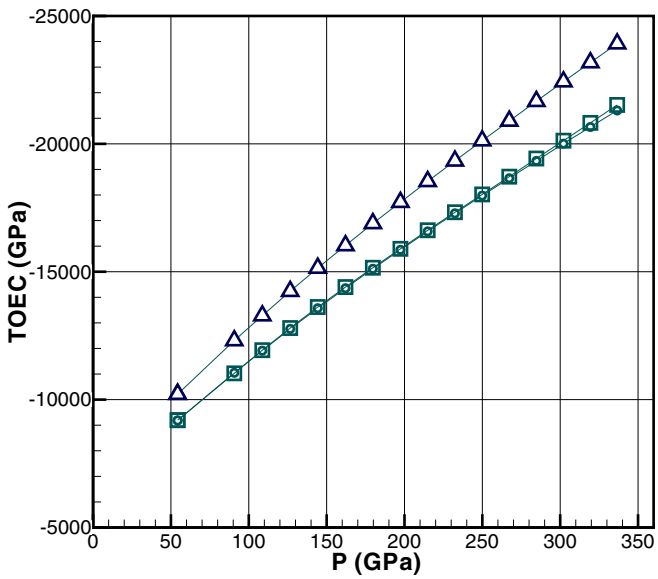

FIG. 3. Pressure dependence of elastic constants $\tilde{C}_{111}$ (triangles), $\tilde{C}_{222}$ (circles), and $\tilde{C}_{333}$ (squares) of *hcp* Fe calculated at $T = 0$ K.

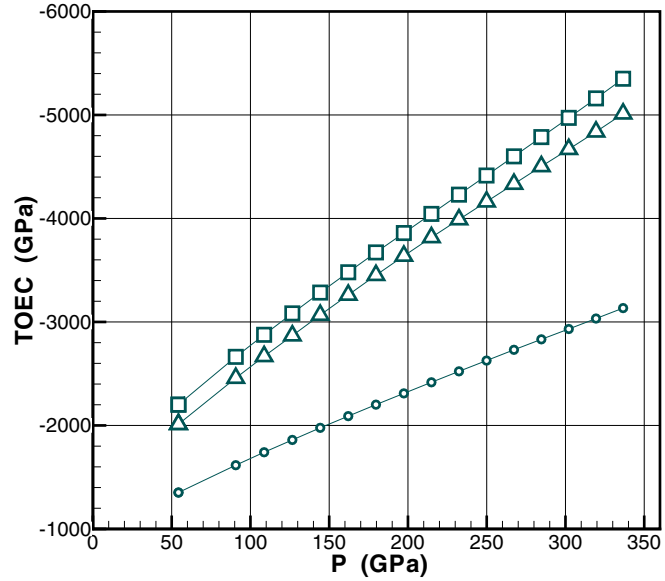

FIG. 4. Pressure dependence of elastic constants $\tilde{C}_{133}$(triangles), $\tilde{C}_{155}$ (circles), and $\tilde{C}_{344}$ (squares) of *hcp* Fe calculated at $T = 0$ K.

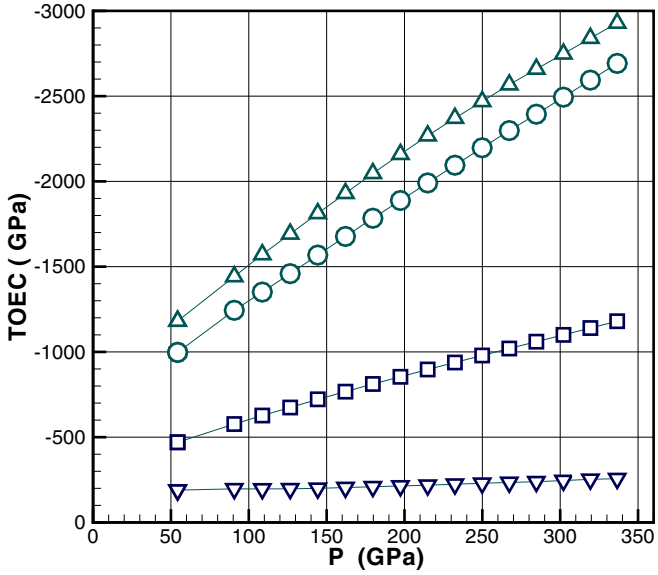

FIG. 5. Pressure dependence of elastic constants $\tilde{C}_{112}$(up triangles), $\tilde{C}_{113}$(circles), $\tilde{C}_{144}$(squares) and $\tilde{C}_{123}$ (down triangles) of *hcp* Fe calculated at $T = 0$ K.

absolute values increase with the increasing pressure. The values of elastic constants $\tilde{C}_{111}$, $\tilde{C}_{222}$, and $\tilde{C}_{333}$ are quite close to each other, though $\tilde{C}_{222}$ is closer to $\tilde{C}_{333}$ than to $\tilde{C}_{111}$. On the other hand, they are almost an order of magnitude larger than the $\tilde{C}_{112}$, $\tilde{C}_{113}$, $\tilde{C}_{133}$, $\tilde{C}_{155}$, and $\tilde{C}_{344}$. The lowest absolute values are calculated for $\tilde{C}_{123}$ and $\tilde{C}_{144}$.

Figure 6 shows the phonon dispersion relations of *hcp*-Fe calculated at $P = 75$ GPa and $P = 300$ GPa. We do not observe any softening of the phonon branches in the given pressure interval, and with increasing pressure the phonon spectrum behaves in a usual way (it becomes "harder"). These facts confirm the stability of the hcp structure of iron in the investigated pressure interval at low temperatures. It is seen that at $P = 75$, as well as at $P = 300$ GPa the acoustic

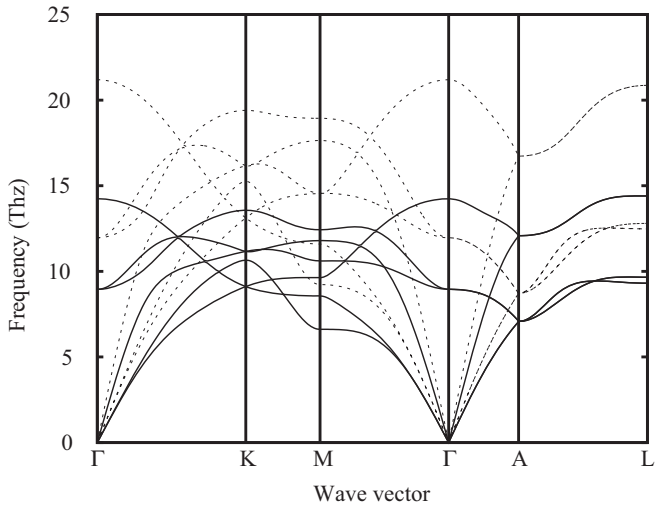

FIG. 6. Phonon dispersion relations of hcp Fe along high symmetry directions. Solid line shows results calculated at $P = 75$ GPa, dashed line is for $P = 300$ GPa.

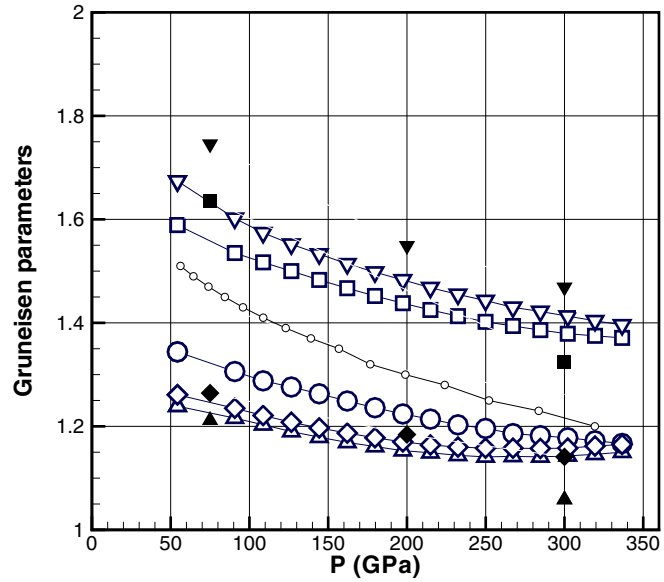

FIG. 7. Pressure dependence of long-wave acoustic modes Grüneisen parameters. Up triangles, diamonds, and circles are the transverse modes with [001]/[100], [100]/[001], and [100]/[010] propagation directions/polarizations, respectively, Squares and down triangles are the longitudinal modes [001], [100]. Open symbols show the GPs calculated from elastic constants. Filled symbols show the GPs derived from the phonon frequencies. Open points denote experimental results for the Grüneisen parameter averaged over all the acoustic branches of the vibrational spectrum γ_v, the experimental error is ± 0.1, see Refs. [47,48].

branches of the transverse vibrations for the Γ-K and Γ-*M* directions are practically degenerate near the BZ centrum.

Using the SOECs and TOECs data for a compressed ε-Fe, we calculated the pressure dependence of Grüneisen parameters (GPs) for the long-wave longitudinal and transverse acoustic modes, propagating along the sixfold axis, as well as in the perpendicular plane. They are defined as [39]

$$\gamma_j = -(V_0/\omega_j)(d\omega_j/dV)_P, \tag{10}$$

where ω_j is frequency of j-th normal vibrational mode. γ_j is determined by the volume change of ω_j and characterizes the lattice anharmonicity. Thermodynamic Grüneisen parameter γ is a weighted average of the γ_j ($\gamma = \sum \gamma_j C_{jv} / \sum C_{jv}$, where C_{jv} is the heat capacity associated with the mode j and frequency ω_j at constant volume).

The general expression for γ_j of a crystal with arbitrary symmetry at zero pressure is given in Eq. (12) of Ref. [45]. The GPs are expressed via the elastic constants defined in Eq. (5) for unloaded crystal. In our case when the crystal is under hydrostatic pressure, $C_{\alpha\beta..}$ Eq. (12) of [45] should be replaced by $\tilde{C}_{\alpha\beta..}$ defined in Eq. (3). The obtained expression for the *hcp* crystal is given in Appendix C [Eq. (C1)].

In Fig. 7 the GPs for long-wave acoustic modes propagating in the high symmetry directions (along the sixfold axis and in the perpendicular plane) are shown. The transverse waves are as follows: (i) for propagation direction [001] and polarization [100] velocity $\upsilon_1 = \sqrt{\tilde{C}_{44}/\rho}$; (ii) for propagation direction [100] and polarization [010] velocity

$\upsilon_2 = \sqrt{(\tilde{C}_{11} - \tilde{C}_{12})/2\rho}$; (iii) for propagation direction [100] and polarization [001] velocity $\upsilon_3 = \sqrt{\tilde{C}_{44}/\rho}$. The longitudinal waves are as follows: (iv) for propagation direction [001] velocity $\upsilon_4 = \sqrt{\tilde{C}_{33}/\rho}$; (v) for propagation direction [100] velocity $\upsilon_5 = \sqrt{\tilde{C}_{11}/\rho}$. In the expressions above ρ denotes the density of the material at the corresponding pressure.

One can see that the GPs of *hcp* Fe for the longitudinal modes exceed those for the transverse modes. The vibrational frequencies increase with increasing pressure (Fig. 7), and this also demonstrates that the lattice is dynamically stable in the studied pressure interval. However, at high pressures this increase slows down, and with further pressure increase the softening of the transverse modes frequencies would occur first.

In Refs. [47,48] the experimental values of the vibrational GP averaged over all the acoustic branches of the vibrational spectrum γ_v for *hcp*-Fe have been obtained in the pressure interval 0–330 GPa ($T = 300$ K). This was done by measuring the intensity change of x-ray diffraction lines upon compression. As a result, the Debye temperature θ was obtained as a function of V/V_0. From the Debye relationship, $\gamma_v = -(\partial \ln\theta/\partial \ln V)_T$, the experimental data on γ_v versus P were determined. The results are shown in Fig. 7. The experimental data in the investigated pressure range is determined with an error ± 0.1 [47]. Taking into account the fact that γ_v is the average value, we conclude that our calculated results are in good agreement with the experimental data and show the same tendency to decrease with increasing pressure.

The GPs have also been calculated from the volume dependence of the phonon frequencies at selected pressures as

$$\gamma_j = -\frac{V_0}{\omega_j}\frac{d\omega_j}{dV} \approx -\frac{1}{2}\frac{V_0}{\omega_j}\left[\frac{\omega_j(V_0) - \omega_j(V_0 - 0.01V_0)}{0.01V_0} + \frac{\omega_j(V_0 + 0.01V_0) - \omega_j(V_0)}{0.01V_0}\right], \tag{11}$$

where V_0 is the volume at the corresponding pressure, ω_j is the frequency of j-th normal vibrational mode with the corresponding wave vector and the polarization, and $\omega_j(V_0 \pm 0.01V_0)$ are the frequencies at the volumes corresponding to $\pm 1\%$ deviation from the original volume. The obtained results are shown in Fig. 7 for comparison with GPs calculated from the elastic constants. The agreement between the two sets is satisfactory.

VI. CONCLUSION

We studied the nonlinear elastic properties of the epsilon phase of iron in the pressure range 50–340 GPa. We preformed *ab initio* DFT calculations of the second and the third order elastic constants. The obtained results for the third order elastic constants may be used for the interpretation of x-ray diffraction data at nonhydrostatic pressure. We derived the expressions for the long-wave acoustic modes Grüneisen parameters for *hcp* structures in terms of the second and third order elastic constants and calculated these parameters for longitudinal and transverse acoustic modes for high-symmetry directions in the considered pressure interval. In addition, we have calculated the phonon dispersion relations and Grüneisen parameters for the corresponding acoustic modes directly from the volume dependence of vibrational frequencies obtained in quasiharmonic approximation. Our results demonstrate that *hcp* iron remains stable in the studied pressure interval and at low temperatures.

ACKNOWLEDGMENTS

Calculations of elastic properties were supported by the Russian Science Foundation (Project No. 18-12-00492). Support from the Swedish Research Council (V.R.) through project Grant No. 2015–04391 is gratefully acknowledged.

APPENDIX A: DEPENDENCE OF FREE ENERGY ON DEFORMATION FOR THE *hcp* LATTICE

Let us consider Eq. (6). For $\Delta F_1/V_0$ we obtain

$$\frac{\Delta F_1}{V_0} = -P(\eta_1 + \eta_2 + \eta_3). \tag{A1}$$

Here and below components of the Lagrangian strain tensor η_α are given in Voigt notations: $11 \to 1$, $22 \to 2$, $33 \to 3$, $23 \to 4$, $13 \to 5$, $12 \to 6$. The expressions for the others two terms in Eq. (6) depend on crystal symmetry. The crystals with the hexagonal symmetry (groups 622, $6/mmm$, $\bar{6}m2$, and $6mm$) have five SOECs $C_{\alpha\beta}$ and ten TOECs $C_{\alpha\beta\gamma}$ [19]. The elastic constants are given in Voigt notations. Using the results of Refs. [28,29] we present the relations $\Delta F_2/V_0$ and $\Delta F_3/V_0$ for the hcp crystal in the following form:

$$\Delta F_2/V_0 = \tfrac{1}{2}C_{11}\left(\eta_1^2 + \eta_2^2\right) + C_{12}\eta_1\eta_2 + \tfrac{1}{4}(C_{11} - C_{12})\eta_6^2 + C_{13}(\eta_1\eta_3 + \eta_2\eta_3) + \tfrac{1}{2}C_{44}\left(\eta_4^2 + \eta_5^2\right) + \tfrac{1}{2}C_{33}\eta_3^2, \tag{A2}$$

$$\begin{aligned}\Delta F_3/V_0 = {} & C_{111}\left(\tfrac{1}{6}\eta_1^3 + \tfrac{1}{2}\eta_2^2\eta_1 - \tfrac{1}{4}\eta_1\eta_6^2 + \tfrac{1}{4}\eta_2\eta_6^2\right) + C_{112}\left(\tfrac{1}{2}\eta_1^2\eta_2 + \tfrac{1}{2}\eta_2^2\eta_1 - \tfrac{1}{8}\eta_1\eta_6^2 - \tfrac{1}{8}\eta_2\eta_6^2\right) \\ & + C_{113}\left(\tfrac{1}{2}\eta_1^2\eta_3 + \tfrac{1}{2}\eta_2^2\eta_3 + \tfrac{1}{4}\eta_3\eta_6^2\right) + C_{123}\left(\eta_1\eta_2\eta_3 - \tfrac{1}{4}\eta_3\eta_6^2\right) + \tfrac{1}{2}C_{133} \\ & \times \eta_3^2\left(\eta_1 + \eta_2\right) + \tfrac{1}{2}C_{144}\left(\eta_1\eta_4^2 + \eta_2\eta_5^2 - \eta_4\eta_5\eta_6\right) + \tfrac{1}{2}C_{155}\left(\eta_2\eta_4^2 + \eta_1\eta_5^2 + \eta_4\eta_5\eta_6\right) \\ & + C_{222}\left(\tfrac{3}{8}\eta_1\eta_6^2 + \tfrac{1}{6}\eta_2^3 - \tfrac{1}{2}\eta_2^2\eta_1 - \tfrac{1}{8}\eta_2\eta_6^2\right) + \tfrac{1}{6}C_{333}\eta_3^3 + \tfrac{1}{2}C_{344}\left(\eta_3\eta_4^2 + \eta_3\eta_5^2\right).\end{aligned} \tag{A3}$$

Here $C_{\alpha\beta}$ and $C_{\alpha\beta\gamma}$ are formally defined in Eq. (5) but the derivatives are calculated at volume V_0 corresponding to the pressure P.

APPENDIX B: DEPENDENCE OF J ON DEFORMATION

Using Eq. (8), we present the Jacobian of the variables r_i with respect to the variable R_j as the sum of terms up to the third power of η_{ij} :

$$J - 1 = J_1 + J_2 + J_3, \tag{B1}$$

$$J_1 = \eta_1 + \eta_2 + \eta_3, \tag{B2}$$

$$J_2 = \eta_1\eta_2 + \eta_1\eta_3 + \eta_2\eta_3 - \tfrac{1}{2}\big(\eta_1^2 + \eta_2^2 + \eta_3^2 + \eta_4^2 + \eta_5^2 + \eta_6^2\big), \tag{B3}$$

$$\begin{aligned} J_3 = {} & \eta_1\eta_2\eta_3 + \eta_4\eta_5\eta_6 + \tfrac{1}{2}\big(\eta_1^3 + \eta_2^3 + \eta_3^3 + \eta_3\eta_5^2 - \eta_1\eta_2^2 - \eta_1\eta_3^2 - \eta_1\eta_4^2 + \eta_1\eta_5^2 \\ & + \eta_1\eta_6^2 - \eta_2\eta_3^2 + \eta_2\eta_4^2 - \eta_1^2\eta_2 - \eta_1^2\eta_3 - \eta_2^2\eta_3 - \eta_2\eta_5^2 + \eta_2\eta_6^2 + \eta_3\eta_4^2 - \eta_3\eta_6^2\big). \end{aligned} \tag{B4}$$

APPENDIX C: GRÜNEISEN PARAMETERS OF LONG WAVE ACOUSTIC MODES FOR *hcp* CRYSTAL

Consider the vibrational mode with unit vector $\vec{N} = \{N_1, N_2, N_3\}$ in the direction of propagation and with the unit polarization vector $\vec{U} = \{U_1, U_2, U_3\}$. For a crystal with *hcp* symmetry, using Eq. (12) of [45], we have

$$\begin{aligned} \gamma_j = -\frac{1}{2Kw}\big\{ & 1 + 2w \cdot \big[(\tilde{S}_{11} + \tilde{S}_{12})\big(U_1^2 + U_2^2\big) + \tilde{S}_{13}\big(1 + U_3^2\big) + \tilde{S}_{33}U_3^2\big] + (\tilde{S}_{11} + \tilde{S}_{12} + \tilde{S}_{13}) \\ & \times \big[(\tilde{C}_{111} + \tilde{C}_{112})N_1^2U_1^2 + 2(\tilde{C}_{112} + \tilde{C}_{122})N_1N_2U_1U_2 + 2(\tilde{C}_{123} + \tilde{C}_{113})(N_1N_3U_1U_3 + N_2N_3U_2U_3) \\ & + (\tilde{C}_{122} + \tilde{C}_{222})N_2^2U_2^2 + 2\tilde{C}_{133}N_3^2U_3^2 + \tilde{C}_{166}(N_1U_2 + N_2U_1)^2 + (\tilde{C}_{144} + \tilde{C}_{155}) \\ & \times\big[(N_1U_3 + N_3U_1)^2 + (N_2U_3 + N_3U_2)^2\big] + \tilde{C}_{266}(N_1U_2 + N_2U_1)^2\big] + (\tilde{S}_{33} + 2\tilde{S}_{23}) \\ & \times \big[\tilde{C}_{113}\big(N_1^2U_1^2 + N_2^2U_2^2\big) + \tilde{C}_{333}N_3^2U_3^2 + 2\tilde{C}_{123}N_1N_2U_1U_2 + 2\tilde{C}_{133}(N_1N_3U_1U_3 + N_2N_3U_2U_3) \\ & + \tilde{C}_{366}(N_1U_2 + N_2U_1)^2 + \tilde{C}_{344}[(N_1U_3 + N_3U_1)^2 + (N_2U_3 + N_3U_2)^2]\big]\big\}. \end{aligned} \tag{C1}$$

Here $w = \rho\upsilon^2$. ρ is the crystal density, υ is the sound velocity in the direction $\vec{N}$ with polarization $\vec{U}$:

$$\begin{aligned} w = {} & \tilde{C}_{11}\big(N_1^2U_1^2 + N_2^2U_2^2\big) + 2\tilde{C}_{12}N_1N_2U_1U_2 + 2\tilde{C}_{13}(N_1N_3U_1U_3 + N_2N_3U_2U_3) + \tilde{C}_{33}N_3^2U_3^2 \\ & + \tilde{C}_{44}[(N_2U_3 + N_3U_2)^2 + (N_1U_3 + N_3U_1)^2] + \tilde{C}_{66}(N_1U_2 + N_2U_1)^2. \end{aligned} \tag{C2}$$

$K = \frac{\tilde{C}_{11}+\tilde{C}_{12}+2\tilde{C}_{33}-4\tilde{C}_{13}}{\tilde{C}_{33}(\tilde{C}_{11}+\tilde{C}_{12})-2\tilde{C}_{13}^2}$ is the volume compressibility [39].

The compliances $\tilde{S}_{\alpha\beta}$ are connected with the elastic constants by the following relations [46]:

$$\begin{aligned} \tilde{S}_{11} &= \frac{\tilde{C}_{11}\tilde{C}_{33} - \tilde{C}_{13}^2}{(\tilde{C}_{11} - \tilde{C}_{12})\big[2\tilde{C}_{13}^2 - \tilde{C}_{33}(\tilde{C}_{11} + \tilde{C}_{12})\big]}, \quad \tilde{S}_{12} = \frac{\tilde{C}_{13}^2 - \tilde{C}_{12}\tilde{C}_{33}}{(\tilde{C}_{11} - \tilde{C}_{12})\big[2\tilde{C}_{13}^2 - \tilde{C}_{33}(\tilde{C}_{11} + \tilde{C}_{12})\big]}, \\ \tilde{S}_{13} &= \frac{\tilde{C}_{13}}{\big[2\tilde{C}_{13}^2 - \tilde{C}_{33}(\tilde{C}_{11} + \tilde{C}_{12})\big]}, \quad \tilde{S}_{33} = \frac{\tilde{C}_{11} + \tilde{C}_{12}}{\tilde{C}_{33}(\tilde{C}_{11} + \tilde{C}_{12}) - 2\tilde{C}_{13}^2}. \end{aligned} \tag{C3}$$

Besides, the additional elastic constants are expressed via the independent $\tilde{C}_{\alpha\beta..}$ [28];

$$\begin{aligned} &\tilde{C}_{66} = (\tilde{C}_{11} - \tilde{C}_{12})/2, \quad \tilde{C}_{122} = \tilde{C}_{111} - \tilde{C}_{222} + \tilde{C}_{112}, \quad \tilde{C}_{166} = \tfrac{3}{4}\tilde{C}_{222} - \tfrac{1}{2}\tilde{C}_{111} - \tfrac{1}{4}\tilde{C}_{112}, \\ &\tilde{C}_{266} = \tfrac{1}{2}\tilde{C}_{111} - \tfrac{1}{4}\tilde{C}_{222} - \tfrac{1}{4}\tilde{C}_{112}, \quad \tilde{C}_{366} = \tfrac{1}{2}(\tilde{C}_{113} - \tilde{C}_{123}), \quad \tilde{C}_{456} = \tfrac{1}{2}(\tilde{C}_{155} - \tilde{C}_{144}). \end{aligned} \tag{C4}$$

In the above expressions we do not take into account the differences between isothermal and adiabatic elastic constants and compliances because the numerical calculations are done at $T = 0\,\mathrm{K}$.

[1] L. Stixrude and R. E. Cohen, Science **267**, 1972 (1995).

[2] X. Sha and R. E. Cohen, Geophys. Res. Lett. **37**, L10302 (2010).

[3] A. P. Jephcoat, H. K. Mao, and P. M. Bell, J. Geophys. Res. **91**, 4677 (1986).

[4] R. D. Taylor and M. P. Pasternak, J. Appl. Phys. **69**, 6126 (1991).

[5] X. Song, Rev. Geophys. **35**, 297 (1997).

[6] K. Glazyrin, L. V. Pourovskii, L. Dubrovinsky, O. Narygina, C. McCammon, B. Hewener, V. Schünemann, J. Wolny, K. Muffler, A. I. Chumakov, W. Crichton, M. Hanfland, V. Prakapenka, F. Tasnádi, M. Ekholm, M. Aichhorn, V. Vildosola, A. V. Ruban, M. I. Katsnelson, and I. A. Abrikosov, Phys. Rev. Lett. **110**, 117206 (2013).

[7] L. Stixrude, Phys. Rev. Lett. **108**, 055505 (2012).
[8] S. Tateno, K. Hirose, Y. Ohishi, and Y. Tatsumi, Science **330**, 359 (2010).
[9] A. K. Singh, H. K. Mao, J. Shu, and R. J. Hemley, Phys. Rev. Lett. **80**, 2157 (1998).
[10] S. Merkel, J. Shu, P. Gillet, H. K. Mao, and R. J. Hemley, J. Geophys. Res. **110**, B05201 (2005).
[11] D. Antonangeli, F. Occelli, H. Requardt, J. Badro, G. Fiquet, M. Krisch, Earth Planet. Sci. Lett. **225**, 243 (2004).
[12] W. L. Mao, V. V. Struzhkin, A. Q. R. Baron, S. Tsutsui, C. E. Tommaseo, H-R. Wenk, M. Y. Hu, P. Ghow, W. Sturhahn, J. Shu, R. J. Hemley, D. L. Heinz, and H-K. Mao, J. Geophys. Res. **113**, B09213 (2008).
[13] S. Merkel, A. F. Goncharov, H.-K. Mao, P. Gillet, and R. J. Hemley, Science **288**, 1626 (2000).
[14] G. Steinle-Neumann, L. Stixrude, and R. E. Cohen, Phys. Rev. B **60**, 791 (1999).
[15] C. Asker, L. Vitos, and I. A. Abrikosov, Phys. Rev. B **79**, 214112 (2009).
[16] L. Vocadlo, D. P. Dobson, and I. G. Wood, Earth Planet. Sci. Lett. **288**, 534 (2009).
[17] X. Sha, and R. E. Cohen, Phys. Rev. B **81**, 094105 (2010).
[18] B. Martorell, J. Brodholt, I. G. Wood, and L. Vocadlo, Earth Planet. Sci. Lett. **365**, 143 (2013).
[19] D. C. Wallace, in *Solid State Physics* (Academic, New York, 1970), Vol. 25, p.301.
[20] Y. Hiki, Ann. Rev. Mater. Sci. **11**, 51 (1981).
[21] O. V. Rudenko, and S. I. Soluyan, *Theoretical Foundations of Nonlinear Acoustics* (Translated from Russian), Plenum, Consultants Bureau, New York, 1977).
[22] J. H. Cantrell, Jr., Phys. Rev. B **21**, 4191 (1980).
[23] Yu. Kh. Vekilov, O. M. Krasilnikov, A. V. Lugovskoy, and Yu. E. Lozovik, Phys. Rev. B **94**, 104114 (2016).
[24] I. Yu. Mosyagin, A. V. Lugovskoy, O. M. Krasilnikov, Yu. Kh. Vekilov, S. I. Simak, and I. A. Abrikosov, Comput. Phys. Commun. **220**, 20 (2017).
[25] G. R. Barsch and Z. P. Chang, J. Appl. Phys. **39**, 3276 (1968).
[26] K. Brugger, Phys. Rev. **133**, A1611 (1964).
[27] T. H. K. Barron and M. L. Klein, Proc. Phys. Soc. **85**, 523 (1965).
[28] A. G. Every and A. K. McCurty, in *Second and Higher order Elastic Constants*, Ladolt-Börnstein, New Series, Group III, Vol. 29a, 639, edited by D.F. Nelson (Springer, Berlin, 1992).
[29] J. K. Liakos and G. A. Saunders, Philos. Mag. A **46**, 217 (1982).
[30] G. Kresse and J. Furthmüller, Phys. Rev. B **54**, 11169 (1996).
[31] J. P. Perdew, J. A. Chevary, S. H. Vosko, K. A. Jackson, M. R. Pederson, D. J. Singh, and C. Fiolhais, Phys. Rev. B. **46**, 6671 (1992).
[32] P. E. Blöchl, Phys. Rev. B **50**, 17953 (1994),
[33] H. J. Monkhorst and J. D. Pack, Phys. Rev. B **13**, 5188 (1976).
[34] M. Methfessel and A. T. Paxton, Phys. Rev. B **40**, 3616 (1989).
[35] P. E. Blochl, O. Jepsen, and O. K. Andersen, Phys. Rev. B **49**, 16223 (1994).
[36] P. Giannozzi, S. Baroni, N. Bonini, M. Calandra, R. Car, C. Cavazzoni, D. Ceresoli, G. L. Chiarotti, M. Cococcioni, I. Dabo, A. Dal Corso, S. de Gironcoli, S. Fabris, G. Fratesi, R. Gebauer, U. Gerstmann, C. Gougoussis, A. Kokalj, M. Lazzeri, L. Martin-Samos, N. Marzari, F. Mauri, R. Mazzarello, S. Paolini, A. Pasquarello, L. Paulatto, C. Sbraccia, S. Scandolo, G. Sclauzero, A. P. Seitsonen, A. Smogunov, P. Umari, and R. M. Wentzcovitch, J. Phys.: Condens. Matter **21**, 395502 (2009).
[37] P. Giannozzi, O. Andreussi, T. Brumme, O. Bunau, M. Buongiorno Nardelli, M. Calandra, R. Car, C. Cavazzoni, D. Ceresoli, M. Cococcioni, N. Colonna, I. Carnimeo, A. Dal Corso, S. de Gironcoli, P. Delugas, R. A. DiStasio Jr, A. Ferretti, A. Floris, G. Fratesi, G. Fugallo, R. Gebauer, U. Gerstmann, F. Giustino, T. Gorni, J. Jia, M. Kawamura, H.-Y. Ko, A. Kokalj, E. Küçükbenli, M. Lazzeri, M. Marsili, N. Marzari, F. Mauri, N. L. Nguyen, H.-V. Nguyen, A. Otero-de-la-Roza, L. Paulatto, S. Poncé, D. Rocca, R. Sabatini, B. Santra, M. Schlipf, A. P. Seitsonen, A. Smogunov, I. Timrov, T. Thonhauser, P. Umari, N. Vast, X. Wu, and S. Baroni, J. Phys.: Condens. Matter **29**, 465901 (2017).
[38] J. P. Perdew, K. Burke, and M. Ernzerhof, Phys. Rev. Lett. **77**, 3865 (1996).
[39] L. Vitos, *Computational Quantum Mechanics for Materials Engineer: The EMTO Method and Applications* (Springer, London, 2007).
[40] M. F. Rose and R. T. Ramsey, Phys. Stat. Solidi B **25**, 103 (1968).
[41] L. V. Pourovskii, J. Mravlje, M. Ferrero, O. Parcollet, and I. A. Abrikosov, Phys. Rev. B **90**, 155120 (2014).
[42] A. Bosak, M. Krisch, A. Chumakov, I. A. Abrikosov, and L. Dubrovinsky, Phys. Earth Planet. Inter. **260**, 14 (2016).
[43] G. Steinle-Neumann, L. Stixrude, R. E. Cohen, and O. Gulseren, Nature (London) **413**, 57 (2001).
[44] J. C. Upadhyaya, D. K. Sharma, D. K. Prakash, and S. C. Upadhyaya, Can. J. Phys. **72**, 61 (1994).
[45] K. Brugger, Phys. Rev. **137**, A1826 (1965).
[46] C. M. Kube and J. A. Turner, J. Elast. **122**, 157 (2016).
[47] O. L. Anderson, L. Dubrovinsky, S. K. Saxena, and T. LeBihan, Geophys. Res. Lett. **28**, 399 (2001).
[48] O. L. Anderson, L. Dubrovinsky, S. K. Saxena, and T. LeBihan, Geophys. Res. Lett. **28**, 2359 (2001).